Multiple Radar Comparison and Analysis of the 8 May 2003 Oklahoma City Tornadic Supercell.

Michael E. Charles
OWC REU
National Weather Service-WFO Norman, OK
SUNY at Stony Brook

Mentors:
David L. Andra, Jr.
Michael P. Foster
Daniel J. Miller
National Weather Service- WFO Norman, OK

Research Experience for Undergraduates Final Project

1 Aug 2003

Abstract

This paper will examine the structure and evolution of the 8 May 2003 Central Oklahoma tornadic supercell using two different radars: the KTLX WSR-88D and the Central Oklahoma TDWR. Measurements of the vertical vorticity and convergence of each of three scales of rotation (mesocyclone, tornado cyclone signature [TCS], and tornadic vortex signature [TVS]) were made by subjectively choosing maximum outbound and inbound velocities from each time/elevation angle of each radar dataset. Data was graphed in the form of time-height plots of mesocyclone and TCS vorticity, and TVS delta-velocity, for both radars. Temporal variation of low-level convergence associated with the supercell was also analyzed.

It was found that the TDWR, with much higher spatial and temporal resolution, was superior to the WSR-88D in resolving the evolution of small-scale storm features. The TCS was always more easily discernable in the TDWR velocity data. The TDWR velocity couplet associated with the TVS tracked very close to the tornado damage path, while the KTLX data was much less accurate at times. The TDWR was also able to resolve one or more surges on the rear-flank downdraft (RFD) that descended into the mesocyclone region and eventually was tied to the development of intense low-level convergence and the TCS. The KTLX WSR-88D did resolve an RFD surge, but it was difficult to track and observe in great detail because of the radar's lower temporal and spatial resolution. The TDWR data was also found to at times be difficult to interpret because of its ability to resolve detailed structures and its tendency to suffer velocity dealiasing failure. Nevertheless, the TDWR was shown to have advantages over the WSR-88D in observing important small-scale storm features.

1. Introduction

Tornadoes and tornadic storms have long been the focus of meteorological research because of the significant threat they pose to life and property. Most of this research focused on supercell thunderstorms, since they produce a significant majority of long-tracked, strong and violent tornadoes. Many observational and theoretical studies of supercell thunderstorms helped build a conceptual model of supercell development and evolution (Lemon and Doswell, 1979). During the past 5-10 years, a significant amount of research focused on the processes within these storms that ultimately lead to tornadogenesis (Markowski et al., 2002).

The defining characteristic of a supercell thunderstorm is a strong, deep, and persistent area of storm-scale rotation called the mesocyclone, which contributes to the high degree of organization and longevity of the storm. Because of the high degree of storm organization, supercells also exhibit other defining features, including a strong, persistent updraft and rear-flank downdraft (RFD). Since radar was developed, it has been used to observe meteorological phenomena, including severe thunderstorms and supercells. The defining features of supercell thunderstorms (mesocyclone, strong updraft, and RFD) often are associated with well defined radar signatures in both reflectivity and velocity data (velocity couplet, bounded weak echo region [BWER], and low-level hook echo) (Browning, 1964). Some tornado-producing supercells exhibit strong, small-scale radar-observed rotational signatures. This feature is known as the tornadic vortex signature (TVS) (Brown et al. 1978). Sometimes an intermediate scale of rotation, smaller than that of the mesocyclone but larger than the TVS, is observed in radar data. This feature was defined as a tornado cyclone signature (TCS), by Magsig et al. (1996).

Lemon and Doswell (1979) also offer a thorough conceptual model of the evolution of a tornadic supercell:

> *The early stages of the mesocyclone evolution are characterized by a strong, rotating updraft and associated BWER. The development of the RFD, which is thought to originate between 4 and 8km AGL, signifies the maturation of the mesocyclone, at which time it evolves into a cyclonically rotating updraft/downdraft couplet. The low-level "hook echo" develops as precipitation is wrapped cyclonically around the upshear flank of the mesocyclone. The descent of the RFD is generally associated with development of a low-level mesocyclone, which may lead to tornadogenesis. Coincident with the descent of the RFD and the development of the low-level hook echo, a TVS sometimes develops, descending from mid-levels to near the ground.*

The primary mission of the National Weather Service (NWS) is the protection of life and property, and inherent in that mission is the forecasting and warning for tornadic thunderstorms. Radar is the most important tool used operationally in the short-term forecast and warning process for severe thunderstorms and tornadoes. A network of weather radars was first deployed in the United States during the 1950s and 1960s (WSR-57 for **W**eather **S**urveillance **R**adar-19**57**), and was upgraded to a national network of Doppler radars (WSR-88D for **W**eather **S**urveillance **R**adar-19**88** **D**oppler) in the 1990s (Crum and Alberty, 1993). Within the past few years, the Federal Aviation Administration's (FAA) Terminal Doppler Weather Radar (TDWR) data has also been

used operationally in a few NWS weather forecast offices (WFOs) as a supplement to data from the WSR-88D radar network.

There are several previous studies of severe storms using higher resolution radar data in supplement to WSR-88D. These studies include Dunn and Vasiloff, (2001), Burgess et al., (2002), and Miller and Burgess, (2003). Burgess et al. (2002) compared radar signatures from the Twin Lakes (KTLX) WSR-88D to those sampled by the Doppler on Wheels (DOW; Wurman et al., 1997) of the 3 May 1999 Oklahoma City tornadic supercell. Dunn and Vasiloff, (2001) examined radar signatures from the KMTX WSR-88D and the Salk Lake City TDWR for the 11 August 1999 Salt Lake City tornado, with emphasis on the velocity signatures prior to and during tornadogenesis. Dunn and Vasiloff, (2001) found that TDWR was superior to the WSR-88D in resolving the small-scale velocity features associated with the tornado, mainly due to sampling limitations of the WSR-88D. Miller and Burgess, (2003) also showed TDWR to be superior to the WSR-88D in spatial and temporal resolution of a microburst in Norman, OK.

During the late afternoon hours of 8 May 2003 supercell thunderstorms developed in central Oklahoma. Although a detailed meteorological analysis is beyond the scope of this paper, Figure 1 shows a 00 UTC (7 PM CDT) 9 May 2003 sounding from Norman, Oklahoma, which best represents the atmosphere near the time of the tornado. This sounding, and other operationally available meteorological data, revealed an environment supportive of supercell storms and tornadoes. One supercell developed southwest of the Oklahoma City, and moved east-northeast across the southern sections of the Oklahoma City metro area through 23 UTC (6 PM CDT), producing a long-track, violent tornado (rated F4 on the Fujita scale) from 2206 UTC (506 PM CDT) to 2236 UTC (536 PM

CDT). This tornado had a path length of approximately 28 km (17 miles), and was responsible for 134 injuries. Both the KTLX WSR-88D and Oklahoma City TDWR sampled this tornadic supercell at close range (generally less than 30km) during the time of the F4 tornado. Figure 2 shows a map of the tornado damage path and the relative locations of both KTLX and TDWR.

This paper will examine radar signatures of the 8 May 2003 Oklahoma City tornadic storm as sampled by the KTLX WSR-88D and the Oklahoma City TDWR. Also included will be discussion of interesting storm-scale features that were observed during the radar data analysis. It will be shown that TDWR was much more successful than KTLX in spatial and temporal resolution of small-scale features. Finally, discussion of the operational implications of these findings will be presented.

2. Data Collection and Methodolgy

Using the beta version of the Warning Decision Support System – Integrated Information (WDSS-II) (Lakshmanan, 2002), velocity and reflectivity data were analyzed for all elevation angles from both KTLX and TDWR between approximately 2130 UTC (430 PM CDT) and 2245 UTC (545 PM CDT). Strengths and limitations of both radars became clearly evident during the data analysis. These strengths and limitations are due to a combination of hardware specifications and the different scanning strategies employed by each radar. Strengths of the WSR-88D include a higher transmitted power and a 10 cm wavelength, that minimize attenuation, a standardized scanning strategy that completes full volume scans every 5 minutes, and data processed by a robust dealiasing algorithm that generally provides the user with easily interpreted velocity data. The

maximum resolution of the WSR-88D is 1.29° effective beam width and a range gate spacing of .25km (Brown and Wood, 1998).

The TDWR transmits at a lower power and 5 cm wavelength, making it much more susceptible to attenuation in areas of heavy rainfall and/or hail. The TDWR uses a volumetric scanning strategy that samples angles from 1° to 28.2° every 6 min., and 0.5° every minute. The smaller Nyquist interval of the 5 cm data presents a challenge to the dealiasing algorithm, which often makes it necessary for the user to manually unfold aliased velocities to properly interpret the data. However, despite these limitations, TDWR has several significant advantages over the WSR-88D. The TDWR has an effective beam width of 1º and gate spacing of .125 km, giving the data superior spatial resolution. In addition, TDWR performs a scan at the 0.5 deg elevation angle once every minute (as opposed to once every 5 minutes by the WSR-88D), providing superior temporal resolution at the lowest levels. Figure 3 shows the velocity signature of the tornado circulation from the perspective of the WSR-88D and the TDWR to compare the resolution of each radar. These images are both at about 2222 UTC (522 PM CDT) and represent a time when the tornado is nearly equidistant to the two radars.

An attempt was made to distinguish three separate scales of rotation observed in the radar data: the mesocyclone scale, TCS (Burgess et al., 2002) scale and the TVS scale (Fig. 4). Low-level convergence was also analyzed. A screen capture of these features was collected for each elevation angle and each time during the evolution of the storm. Each screen capture also contained an overlay of the observed damage path of the tornado as determined by ground damage survey. These screen captures included the three subjectively selected scales of rotation. A line connecting the maximum inbound

and outbound velocities of each feature was drawn, and information about the spatial position and strength of each maximum velocity was recorded (Fig. 4). Screen captures were also made of the lowest angle reflectivity data and overlaid with the tornado damage path.

A spreadsheet was then created containing velocity data from all elevation angles from each radar. Along with information provided in the raw data, several parameters were calculated for each scale of rotation, including rotational velocity (Vrot=deltaV/2) and vorticity (ζ=2*Vrot/R, according to Magsig and Burgess, (1996)). A value of low level convergence was also calculated using the velocity values. These methods were performed for both radar data sets.

Spreadsheet data was imported into Surfer 8, a software package designed to perform objective analysis. Time-height plots of vorticity and rotational velocity (delta-V) for the mesocyclone and TCS, delta-V for the TVS. Convergence was also plotted. Because the objective analysis routines used in Surfer did not accurately portray the evolution of these features, subjective analyses were performed. Plots were created for each radar to compare the datasets.

3. Results

a. Low-level convergence

Both radars show steady convergence in the southeast quadrant of the developing supercell through 2150 UTC (450 PM CDT) (Fig. 5&6). Both also show a general increase in convergence from about 2150 UTC (450 PM CDT) to the time of tornadogenesis (2206 UTC or 506 PM CDT), with an especially rapid increase less than

10 minutes before tornadogenesis (nearly doubles). However, values for convergence were generally higher on TDWR than KTLX (20% higher initially, and 50% higher at tornadogenesis). This was due to the higher spatial and temporal resolution of the small-scale wind fields responsible for low-level convergence and the TDWR being closer to the tornado.

b. Mesocyclone

Both radars detected an organized mesocyclone that was most discernable at around 6-7km AGL, descending from mid-levels to around 1km by tornadogenesis (Fig. 7&8). The mesocyclone, on each radar, developed strongest rotation in the storm's mid-levels, but around 1km lower on TDWR. Peak vorticity (mid-level) occurred nearly 12 minutes earlier on TDWR. The mesocyclone peaked in low-levels between 2224 UTC (524 PM CDT) and 2236 UTC (536 PM CDT) on both radars, but KTLX showed a stronger peak, about $1x10^{-2}$ s^{-1}. After 2224 UTC (524 PM CDT), TDWR depicted a more vertically stratified mesocyclone than KTLX. Peaks mesocyclone vorticity were primarily due to contraction of the mesocyclone.

c. Tornado Cyclone

The tornado cyclone is was determined to be primarily a midlevel circulation on KTLX (Fig. 9). There was little evidence of the tornado cyclone below 2km until around 2221 UTC (521 PM CDT), when vorticity values exceeded $3x10^{-2}$ s^{-1}, some 15 minutes after tornadogenesis. At this time there was a peak in strength in mid-levels ($>6.5x10^{-2}$ s^{-1}). TDWR presented a much different view of the tornado cyclone, however, with the

circulation first observed coincident with tornadogenesis (Fig. 10). The circulation's highest vorticity values are coincident with tornadogenesis as well (nearly $7.5x10^{-2}$ s^{-1}). Close observation of the TDWR 10-15 minutes before tornadogenesis revealed the tornado cyclone developed as the low-level convergence rapidly intensified, becoming more rotational, and finally becoming the tornado cyclone. Significant vorticity associated with the tornado cyclone extended to around 3km AGL (with less significant values upward of 6km AGL), but descended in the first 10 minutes to less than 1km AGL. At around 2218 UTC (518 PM CDT) there was a secondary peak in the tornado cyclone's vorticity (near $4x10^{-2}$ s^{-1}). This time period was well correlated with the time when the tornado was strongest and at its largest extent After this time the tornado cyclone became less discernable and data points were more sparse (though still showing a general weakening in the circulation after the peak at around 2224 UTC [524 PM CDT]).

d. Tornadic Vortex Signature

The TVS was first observed between 2212 UTC (512 PM CDT) and 2215 UTC (515 PM CDT) on KTLX, 6-9 minutes after tornadogenesis, and appeared fairly suddenly throughout the low and mid-levels simultaneously (Fig. 11). In contrast, the TVS developed coincident with the tornado on TDWR (TDWR has the resolution to directly sample the tornado as it developed) *near the surface, and ascended to over 11km AGL within the first 15 minutes of the tornado's lifespan* (Fig. 12). Maximum TVS delta-V occured between 2220 UTC (520 PM CDT) and 2227 UTC (527 PM CDT) on both radars, but values of delta-V are 5-10 m/s lower on KTLX. The strongest near-surface delta-V values occurred at about 2224 UTC (524 PM CDT) on both radars. Significant

TVS delta-V was observed to descend to near the surface by around 2236 UTC (536 PM CDT) on both radars, and each also detected a weakening in mid-levels at around 2230 UTC (530 PM CDT), but about 1km higher on TDWR. The TVS assumed a more vertically stratified structure on both radars at this time, which was more evident on the TDWR. TDWR was able to sample much more of the circulation near the surface because of the temporal/spatial resolution of the radar, and captured many oscillations in strength, the most significant peak in delta-V (nearly 90 m/s) occurring between 2224 UTC (524 PM CDT) and 2227 UTC (527 PM CDT) below 1km AGL. Both radars observed the most developed and intense TVS during the time when the tornado was largest and at its most damaging phase.

4. Other interesting results

a. Shear-maximum track

A comparison was made between the subjectively chosen center of the tornado circulation evident in the lowest elevation angle velocity data and the tornado damage path (Fig. 2). The center of the smallest-scale circulation observed by TDWR exhibited a much better association with the actual path of the tornado, when compared to the smallest-scale circulation observed by KTLX. The track of this feature, observed by TDWR, begins slightly offset from the damage path, but quickly centers on the track, only straying small distances (<0.5km) from the center a few times for the duration of the tornado. In contrast, the center of the smallest-scale circulation observed by KTLX was not centered on the damage path at most times during the tornado. Moreover, the KTLX-

observed feature is often centered outside the observed damage path inconsistently; i.e. sometimes centered on the right of the path, other times on the left.

b. Debris signature

A small "ball" of high reflectivity (> 55 dBz) was evident in data from the lowest elevation slice at the tip of the hook echo during the time of the tornado (Fig. 13). This ball of higher reflectivity was directly associated with debris within the tornado and tornado cyclone circulations. This debris cloud feature developed coincident with tornadogenesis (2206 UTC or 506 PM CDT) in the TDWR data. It can be tracked along the path of the tornado for the entire lifespan of the tornado. Due to the one-minute temporal resolution at the lowest elevation slice, this signature in the TDWR data represents a valuable tornado-detection tool. The debris cloud was also evident in KTLX data, but did not appear until 2216 UTC (516 PM CDT), ten minutes after tornadogenesis. The debris signature from KTLX was also not as well associated with the tornado damage path. The maximum reflectivity value in, and size of, the debris signature from both radars followed the trends in strength and size of the tornado. For example, a marked increase in the maximum reflectivity value and debris cloud size was noted as the tornado impacted the General Motors plant in southeast Oklahoma City and lofted a significantly greater amount of debris.

c. RFD

Several small-scale (< 1km) surges in the RFD were observed beginning about 30 minutes prior to tornadogenesis (Fig. 15). These surges were most apparent on the TDWR, but can be observed at times on KTLX, although in much less spatial and temporal detail. Each small-scale region of higher inbound velocities can be traced back to mid-levels and appears to descend with time. The first of these surges occurred about 30 minutes prior to the tornado, and appeared to penetrate the core of the mid-level mesocyclone/BWER. This maximum inbound velocity associates very well with a developing reflectivity notch on the upshear flank of the mesocyclone, pointing toward the BWER (Fig. 16). This first surge was followed by a second surge further to the south, occurring on the perimeter of the mesocyclone. This second surge (there may be other surges that are more difficult to observe, even with the high resolution TDWR data) was associated with a more defined notch in the reflectivity. This notch preceded the development of the low-level hook echo and coincided very well with the tip of the hook. The surge was traced back more than 20 minutes before tornadogenesis, and ultimately descended to near the surface where it became an area of intense and increasingly rotational convergence. The tornado cyclone then evolved from this region of enhanced convergence.

5. Discussion

The overall evolution of radar-detectable features in the 8 May 2003 Oklahoma City supercell were consistent with the evolution of similar features in previous studies (Lemon and Doswell, 1979; Burgess and Magsig, 1996). The evolution of the

mesocyclone adhered to the conceptual model of a strong mid-level circulation descending with time. The mesocyclone was shown to steadily descend into low-levels, and was closely tied to the tornado cyclone circulation near the time of tornadogenesis. Convergence beneath the mid-level mesocyclone was pronounced and steady as the supercell strengthened, supporting continuing upward motion to maintain the storm. Near tornado time, convergence near the surface significantly increased (nearly doubling), and acquired a rotational component. This was coincident with the mesocyclone developing in low-levels. There was a low-level relative maximum in the strength of the mesocyclone, tornado cyclone and convergence at tornado time. The peak in tornado strength at about 2225 UTC (525 PM CDT) corresponded to an enhancement of the mesocyclone and tornado cyclone in the low to mid-levels. At about 2226 UTC (526 PM CDT) the TVS weakened significantly in mid-levels. This was associated with an increase in the strength of the tornado cyclone in low-levels, and a significant decrease in its strength in mid-levels. It also coincided with an increase in mesocyclone strength.

There were several difficulties found during the analysis of the data, especially TDWR data, that have significant operational implications. Subjectively identifying three scales of circulation was very difficult at times. A tornado cyclone was not even observable at times on KTLX, which most likely led to the significant differences between the KTLX and TDWR time-height plots of tornado cyclone vorticity. The KTLX tornado cyclone time-height plot is thought to be less reliable than the TDWR plot because there were many times when a tornado cyclone was ambiguous or non-existent in the velocity data.

6. Important Operational Implications for TDWR

The TDWR provided superior resolution to the debris cloud that developed coincident with the tornado (Fig. 13). It could be followed throughout the tornado's lifetime, and was highly correlated to the damage. Because this feature occurs on such a small time and spatial scale, the superior resolution of the TDWR (.125km/1min.) is very useful for tornado detection and warning, particularly close to the radar.

The smaller scale circulations (tornado cyclone and TVS) were much more apparent and detailed on TDWR than KTLX. In both reflectivity and velocity, there was detailed structure to the tornado cyclone. It was often associated, in low-levels, with a maximum in reflectivity that surrounded that tornado, and was located (again in low-levels) at the tip of the hook. The TVS was also observed with outstanding detail by the TDWR, especially in the lowest elevation angle (Fig. 14).

TDWR data has twice the resolution of the WSR-88D velocity data and *eight* times the resolution in the reflectivity data. While this can be used by forecasters to significantly increase the quality of forecasts and warnings, operational use of the data may be difficult at first. With the higher resolution comes more noise and complexity. It was found that at times it was very difficult to subjectively choose data points corresponding to a circulation. The data was of such high resolution that many small-scale circulations were visible at times, and discerning which velocities to choose for the three scales studied was difficult.

The Nyquist interval of the TDWR is smaller than that of the WSR-88D, so inherent problems with dealiasing of velocity data may be expected. At times the interval drops even more because the radar automatically optimizes PRF to serve airport

operations, not sampling of more distant storms. This further complicates data analysis because of increased velocity data folding. Furthermore, the dealiasing algorithm experiences frequent failures in high shear regions. For this project, all velocity data was unfolded manually so as to avoid problems with the dealiasing algorithm. Clearly such manual unfolding was difficult, especially without experience. Practice with unfolding such complex data is crucial to operational use of the TDWR.

Acknowledgements

I extend my sincere thanks to Karen Cooper, Kevin Scharfenberg, Valliappa Lakshmanan and Travis Smith, from the National Severe Storms Laboratory (NSSL), for their expertise in solving numerous computer/software related problems, Don Burgess of NSSL for his expertise in helping to interpret radar signatures, Steve Kruckenberg for help with image editing, and Doug Speheger for creating the tornado damage path shape files for use in WDSS-II. Funding for this project came from the Oklahoma Weather Center REU grant NSF 0097651.

References

Brown, R.A., L.R. Lemon, and D.W. Burgess, 1978: Tornado Detection by Pulsed Doppler Radar. Monthly Weather Review: Vol. 106, pp. 29-39.

Browning, Keith A. 1964: Airflow and Precipitation Trajectories Within Severe Local Storms Which Travel to the Right of the Winds. Journal of the Atmospheric Sciences: Vol. 21, No. 6, pp. 634–639.

Burgess, Donald W., M.A. Magsig, J.Wurman, D.C. Dowell, and Y. Richardson, 2002: Radar Observations of the 3 May 1999 Oklahoma City Tornado. Weather and Forecasting: Vol. 17, No. 3, pp. 456–471.

Crum, T.D., and R.L. Alberty, 1993: The WSR-88D and the WSR-88D Operational Support Facility. *Bull. Amer. Meteor. Soc.,* **74**, 1669-1687.

Dunn, Lawrence B., and S.V. Vasiloff, 2001: Tornadogenesis and Operational Considerations of the 11 August 1999 Salt Lake City Tornado as Seen from Two Different Doppler Radars. Weather and Forecasting: Vol. 16, No. 4, pp. 377–398.

Lakshmanan, V., 2002: WDSS-II: An Extensible, Multi-source Meteorological Algorithm Development Interface. *Preprints:* 21st Conference on Severe Local Storms, San Antonio, TX. Amer. Met. Soc., 134-137.

Lemon, Leslie R., C.A. Doswell, 1979: Severe Thunderstorm Evolution and Mesocyclone Structure as Related to Tornadogenesis. Monthly Weather Review: Vol. 107, No. 9, pp. 1184–1197.

Magsig, Michael A., and D.W. Burgess, 1996: A Vorticity and Divergence Analysis Relating to Tornadogenesis As Seen by a WSR-88D Radar. Preprints:18th conference on Severe Local Storms, San Francisco, CA. Amer. Met. Soc., 418-422.

Markowski, Paul M., J.M. Straka, E.N. Rasmussen, 2002: Direct Surface Thermodynamic Observations within the Rear-Flank Downdrafts of Nontornadic and Tornadic Supercells. Monthly Weather Review: Vol. 130, No. 7, pp. 1692-1721.

Miller, Daniel J., and D.W. Burgess, 2003: Terminal Doppler Weather Radar Observations of a Microburst. Preprints: 31st Conference on Radar Meteorology, Seattle, WA. Amer. Met. Soc., in press.

Brown, R. A. and V. T. Wood, 1998: Technique for improving WSR-88D detection of tornadoes. Preprints, 19th Conf. on Severe Local Storms, 14-18, September, Minneapolis, Amer. Meteor. Soc., Boston, 721-724.

Wurman, Joshua, J. Straka, E. Rasmussen, M. Randall, A. Zahrai, 1997: Design and Deployment of a Portable, Pencil-Beam, Pulsed, 3-cm Doppler Radar. Journal of Atmospheric and Oceanic Technology: Vol. 14, No. 6, pp. 1502–1512.

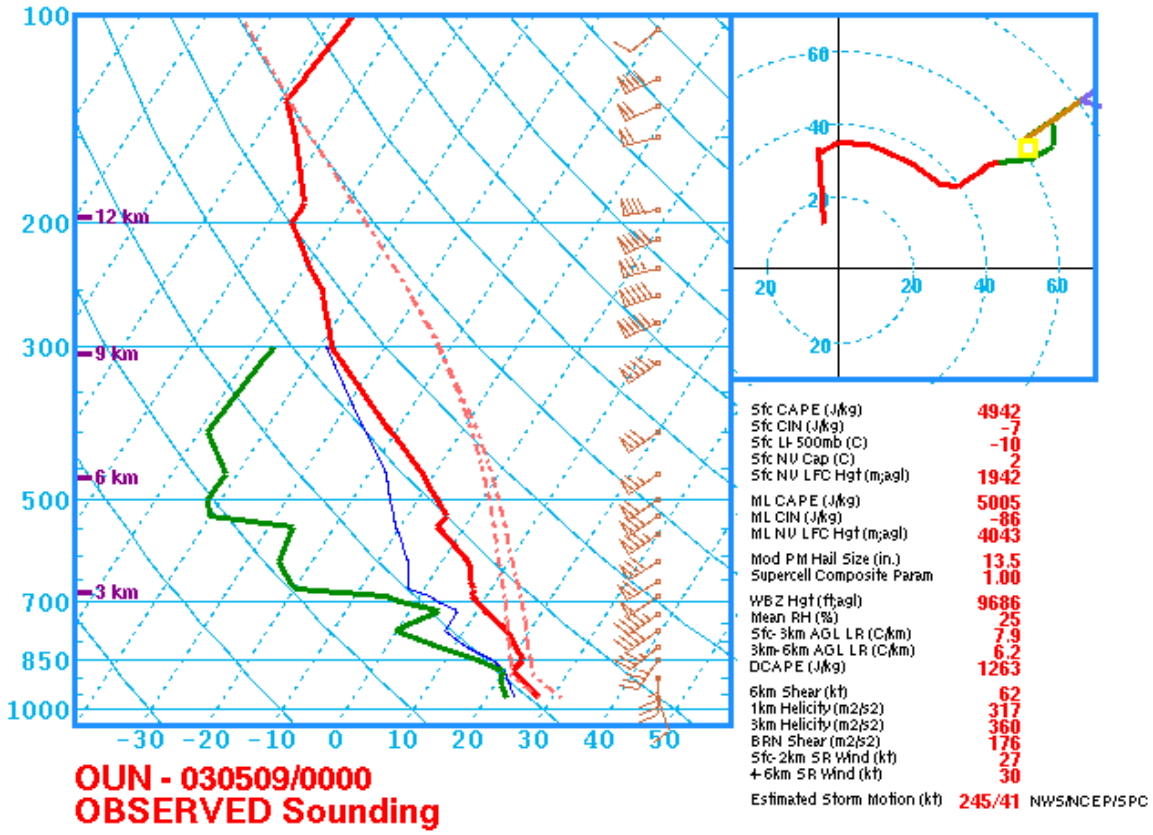

Figure 1. 00z 9 May 2003 sounding and hodograph. This sounding best represents the state of the atmosphere near the time of the tornado.

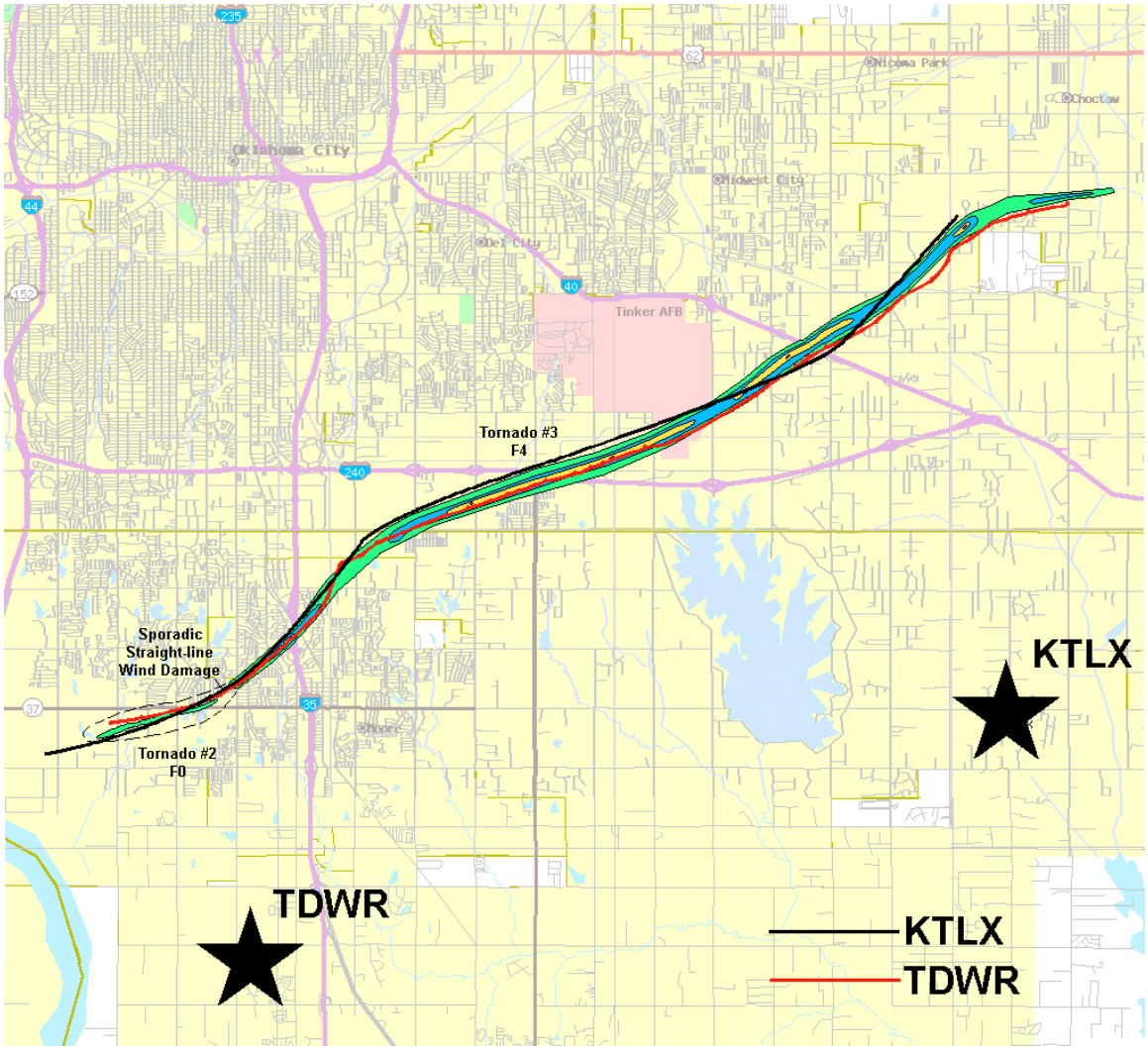

Figure 2. Tornado damage path. Tracks, based on the maximum-shear signature of the tornado circulation as observed by KTLX (black) and TDWR (red), are overlaid. Locations of KTLX and TDWR are denoted by stars.

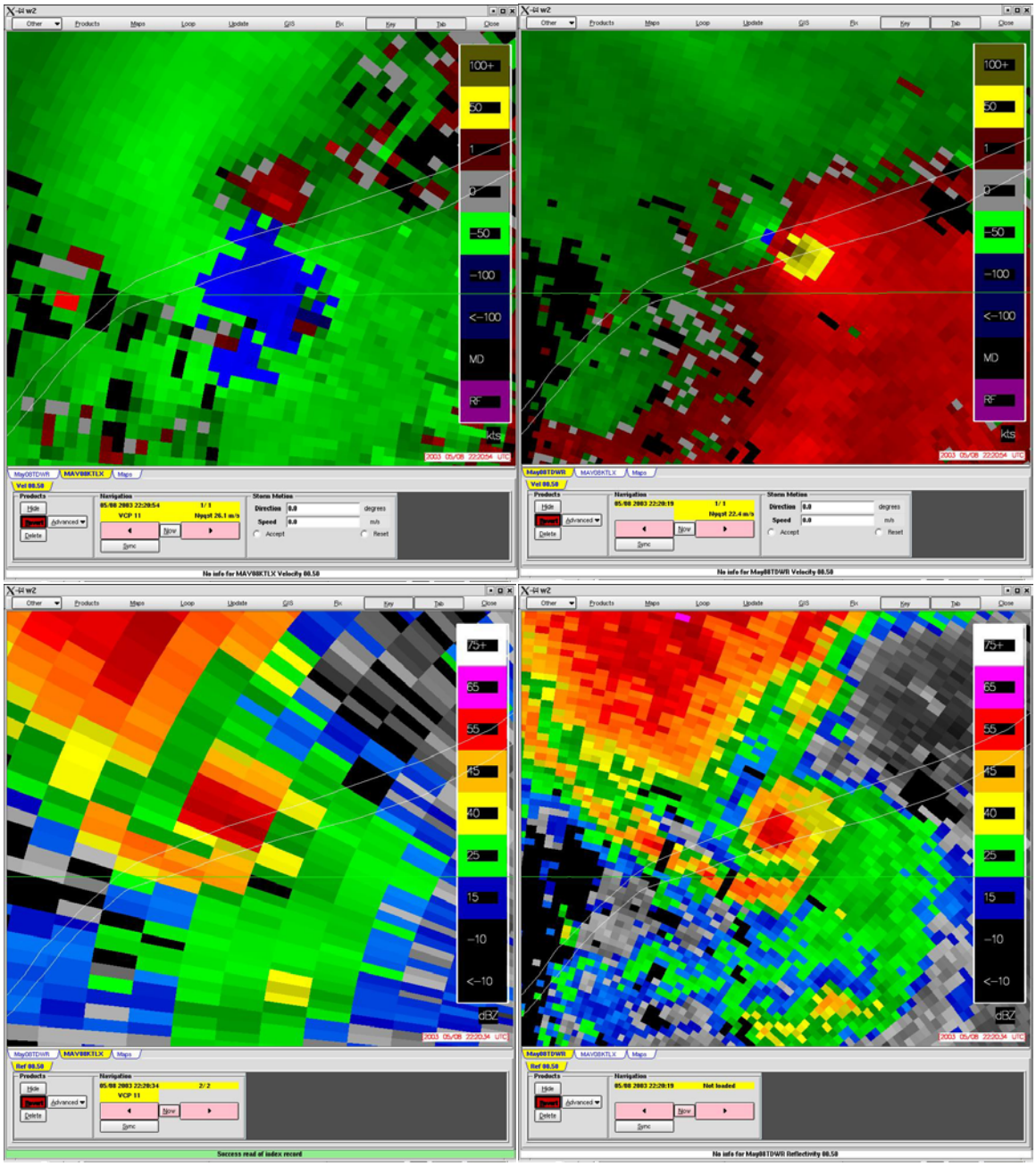

Figure 3. Comparison of WSR-88D (left 2) and TDWR (right 2) spatial resolution in velocity (top 2) and reflectivity (bottom 2) data.

WSR-88D:	Velocity:	1.29° resolution	0.25km range gate spacing
	Reflectivity:	1.29° resolution	1km range gate spacing
TDWR:	Velocity:	1° resolution	125m range gate spacing
	Reflectivity:	1° resolution	125m range gate spacing

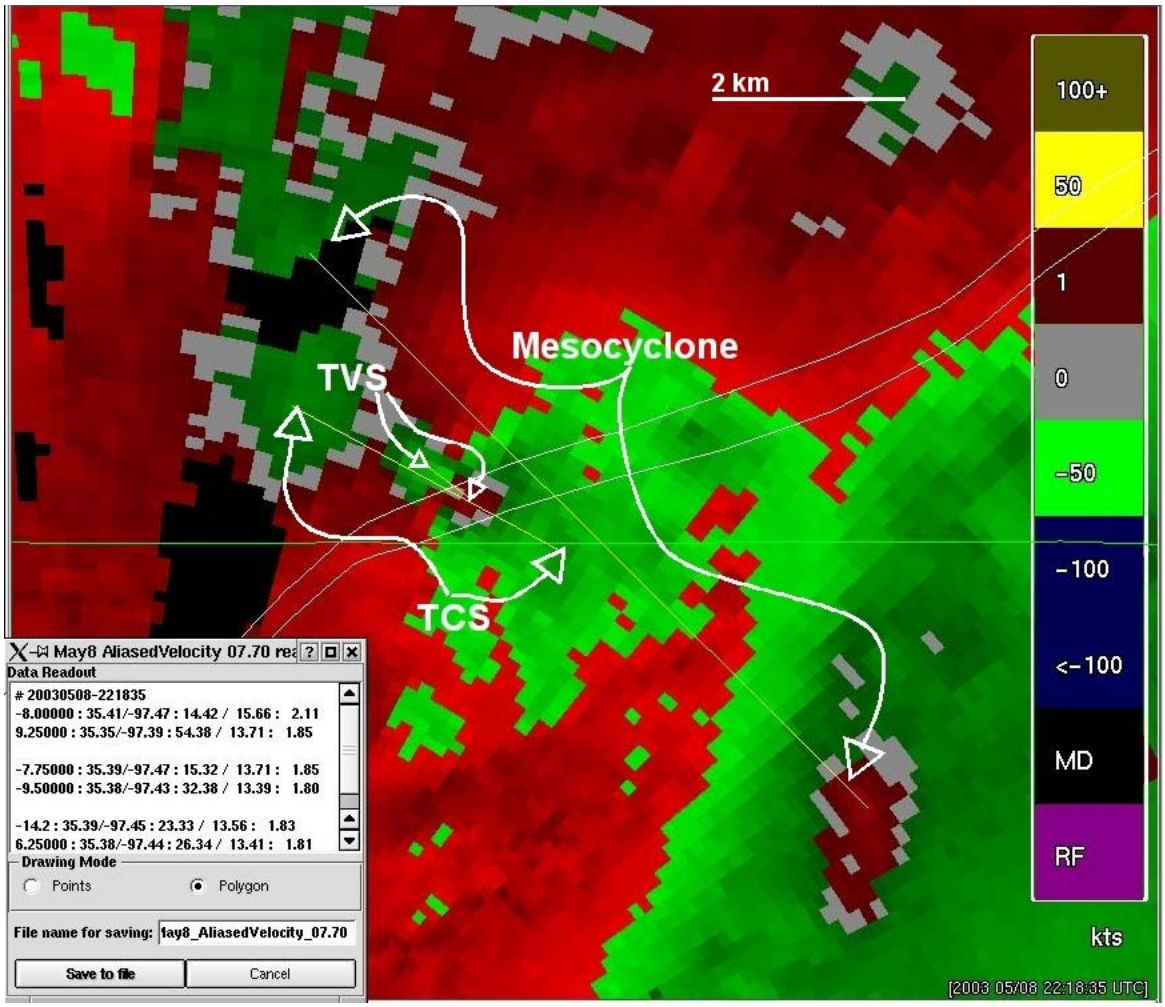

Figure 4. Screen capture of TDWR velocity data containing all three subjectively chosen scales of circulation. Thin yellow lines connect maximum inbound and outbound velocities associated with each circulation, and the data box in the bottom left corner contains information about each velocity data point chosen, including magnitude and position relative to the radar.

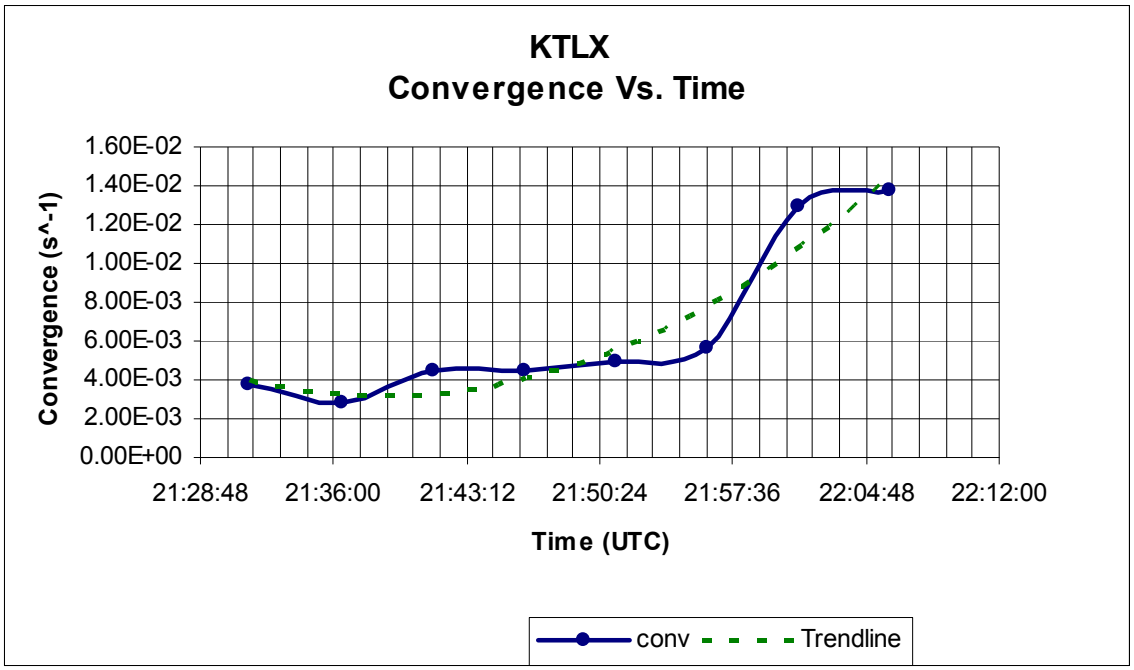

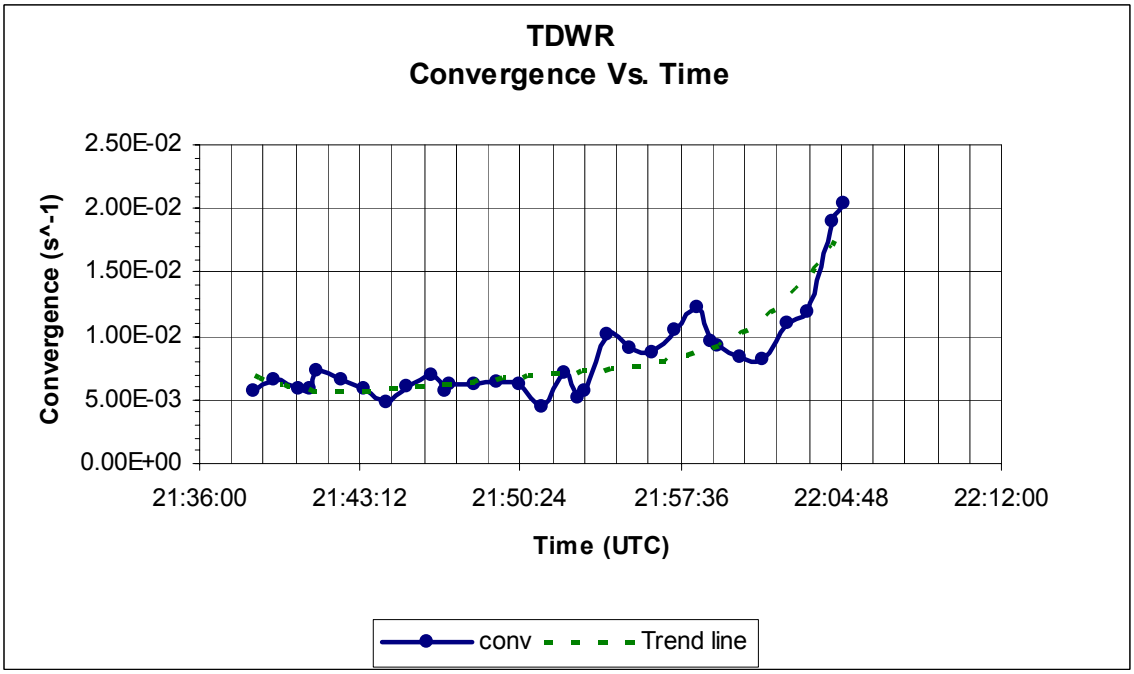

Figures 5 (top) and 6 (bottom). Convergence vs. time at the 0.5° elevation angle for KTLX and TDWR.

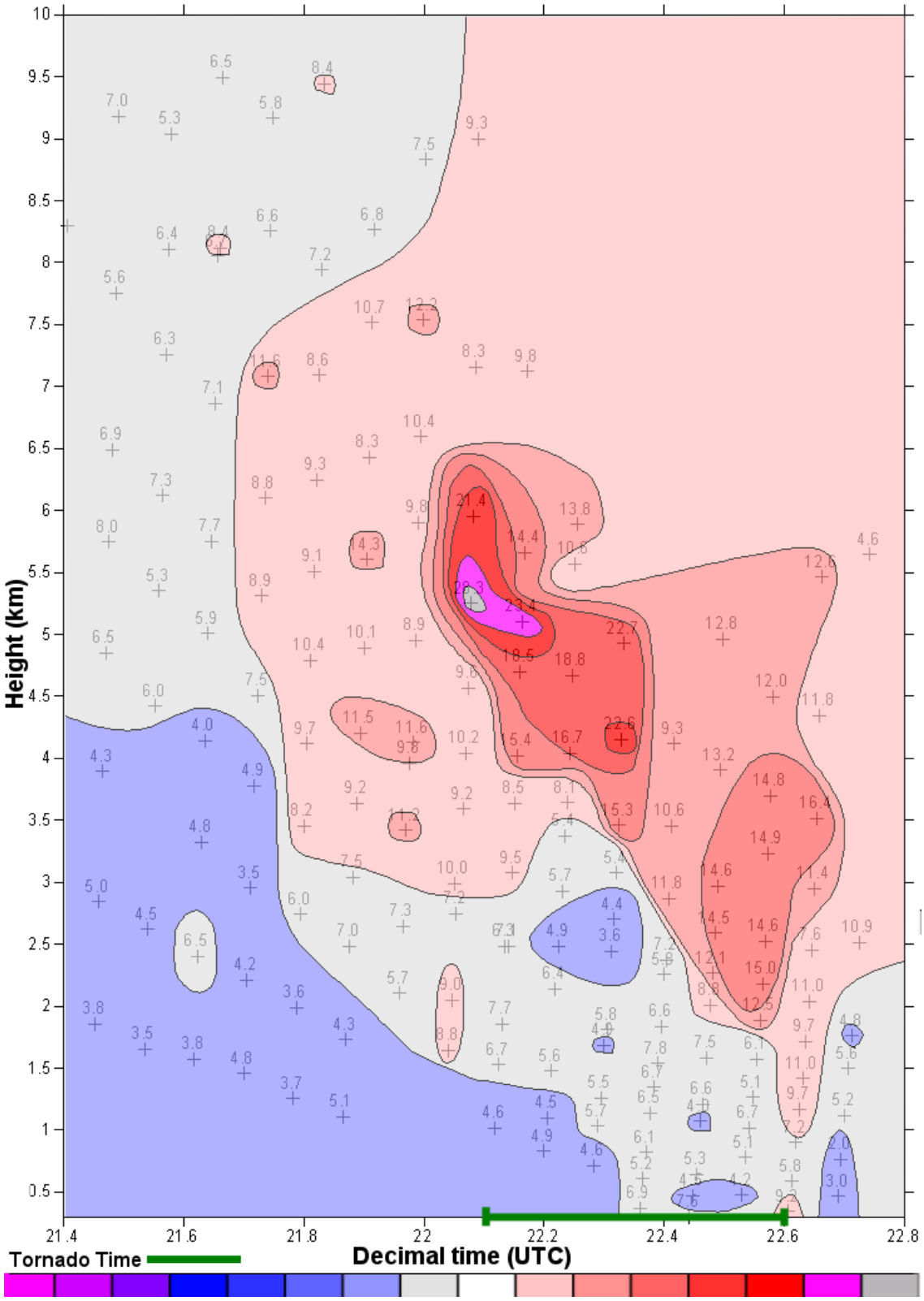

Figure 7. Time-height plot of mesocyclone vorticity ($x10^{-3}$ s^{-1}) from KTLX. Shows mesocyclone descending from mid-levels to low-levels.

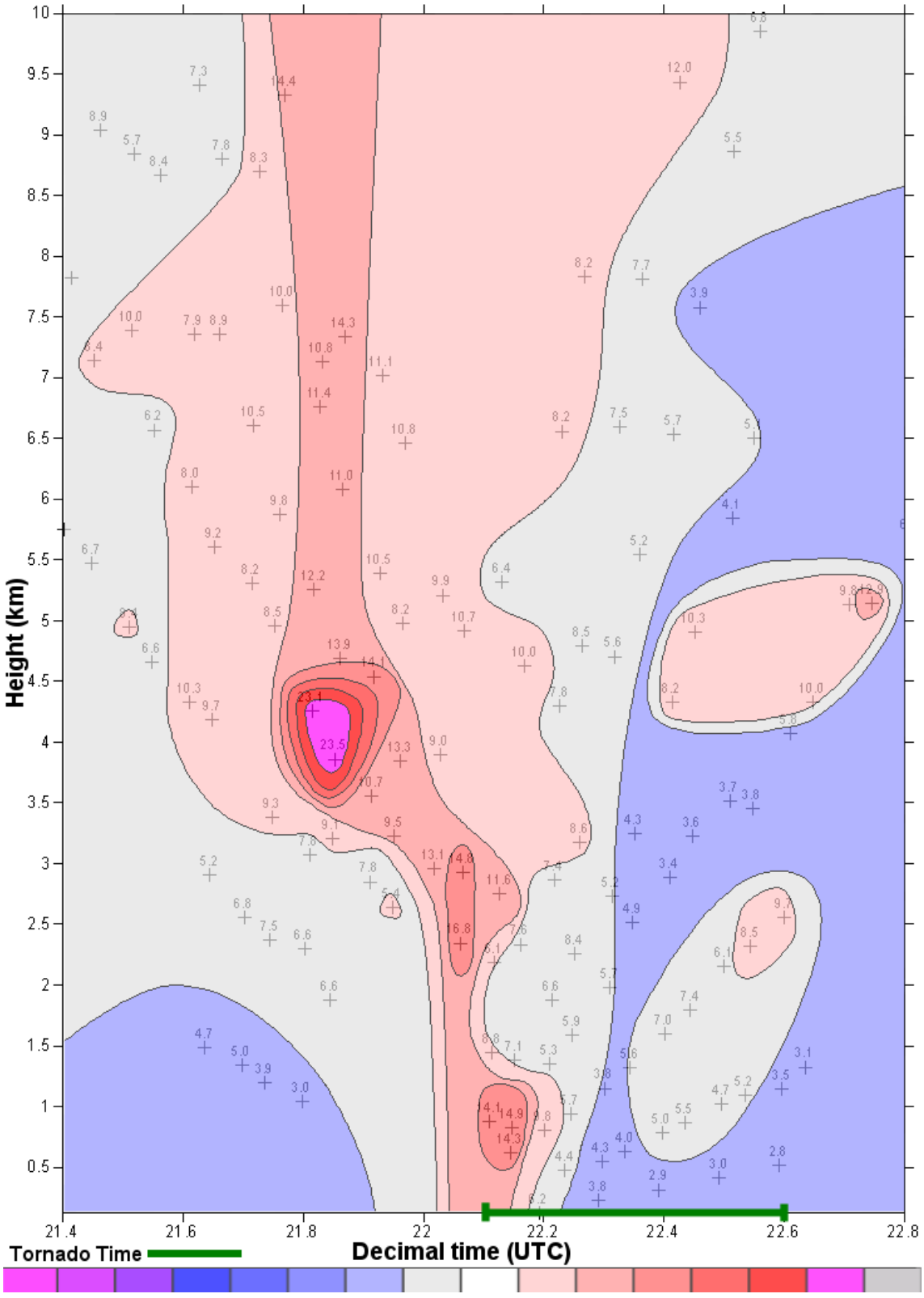

Figure 8. Same as figure 7 but for TDWR.
Shows mesocyclone descending to near the surface by the time of tornadogenesis.

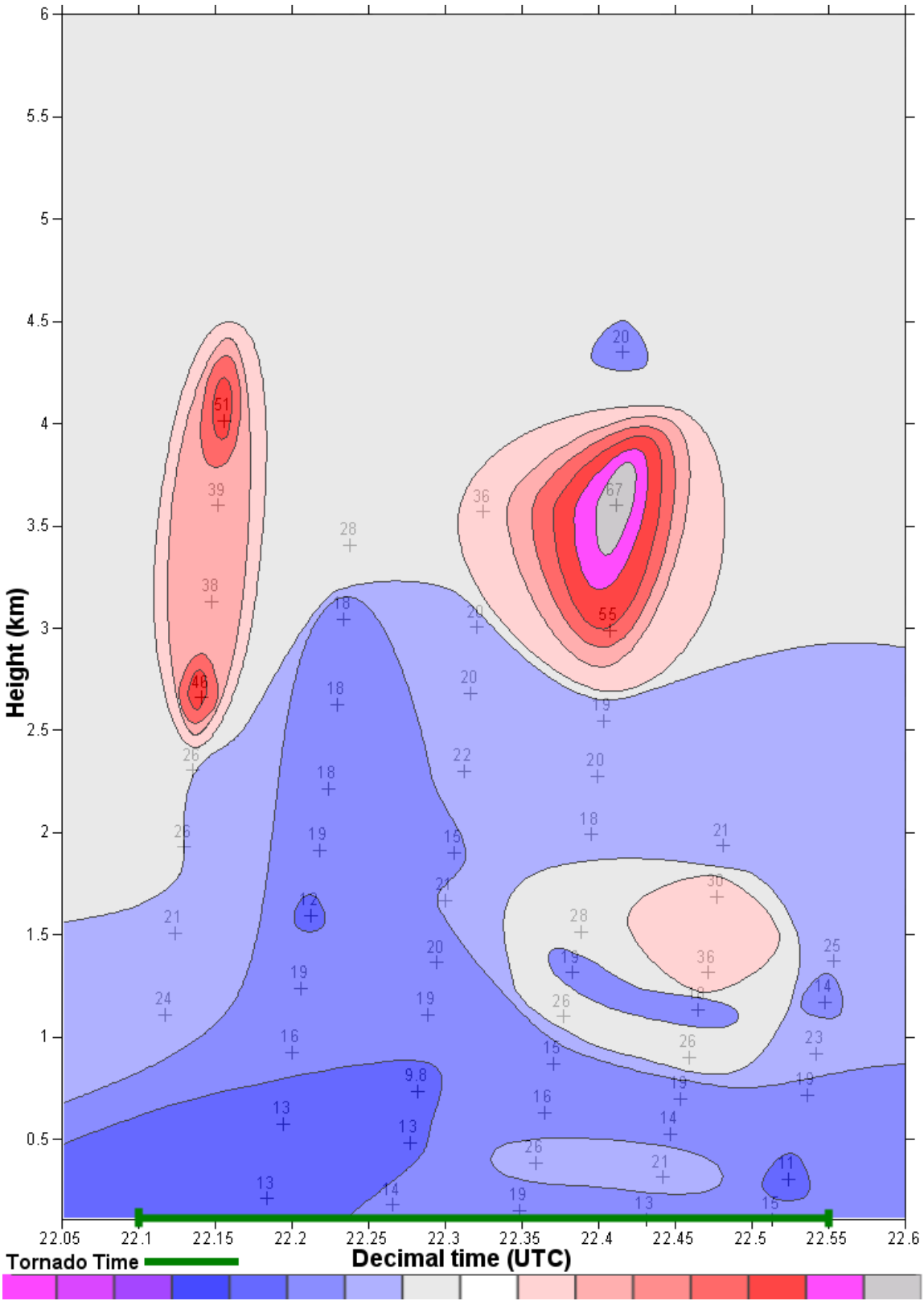

Figure 9. Time-height plot of tornado cyclone vorticity (x10^{-3} s^{-1}) from KTLX. Shows TCS to be a mostly mid-level feature.

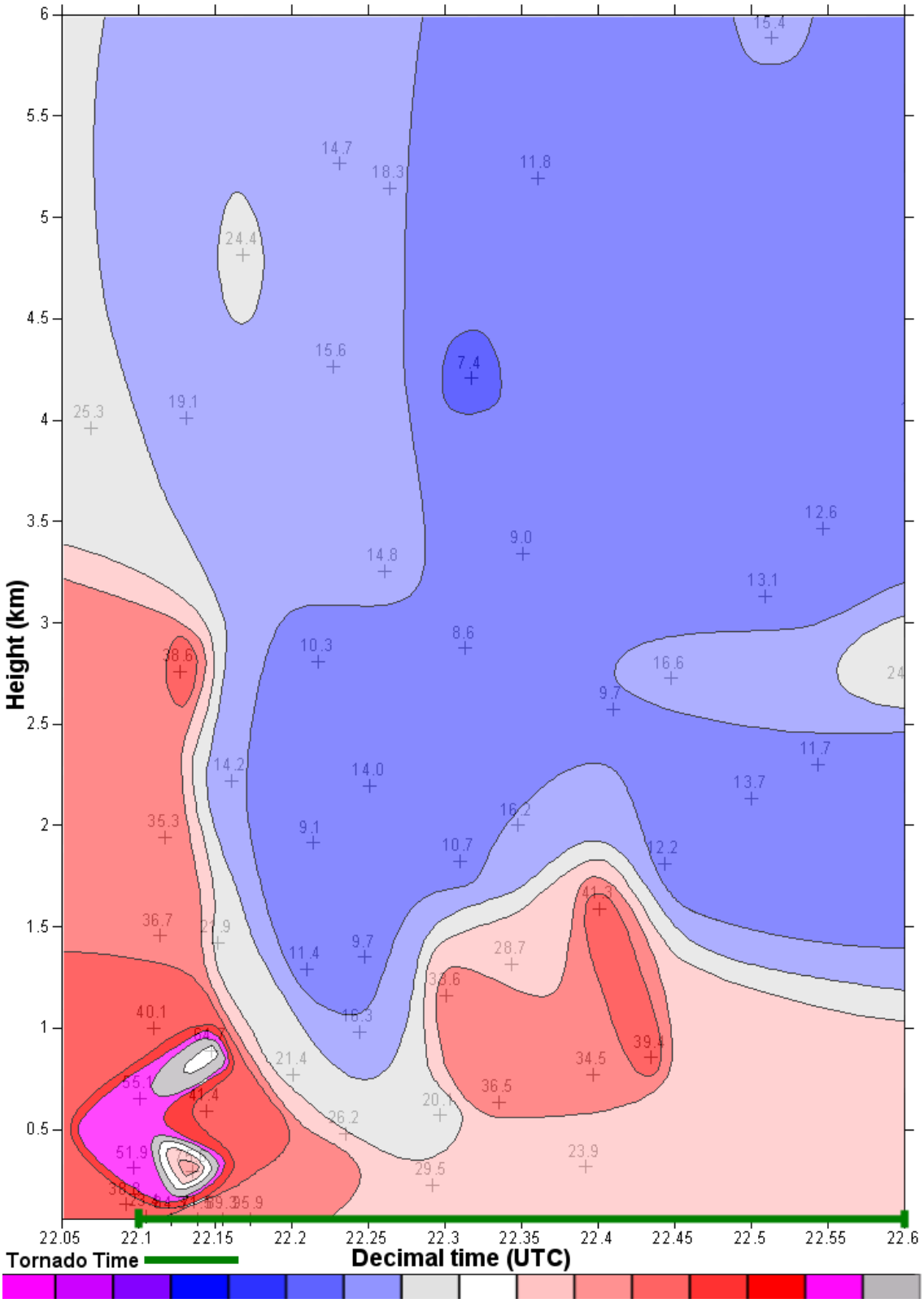

Figure 10. Same as figure 9 but for TDWR.
Shows TCS as mainly a low-level feature.

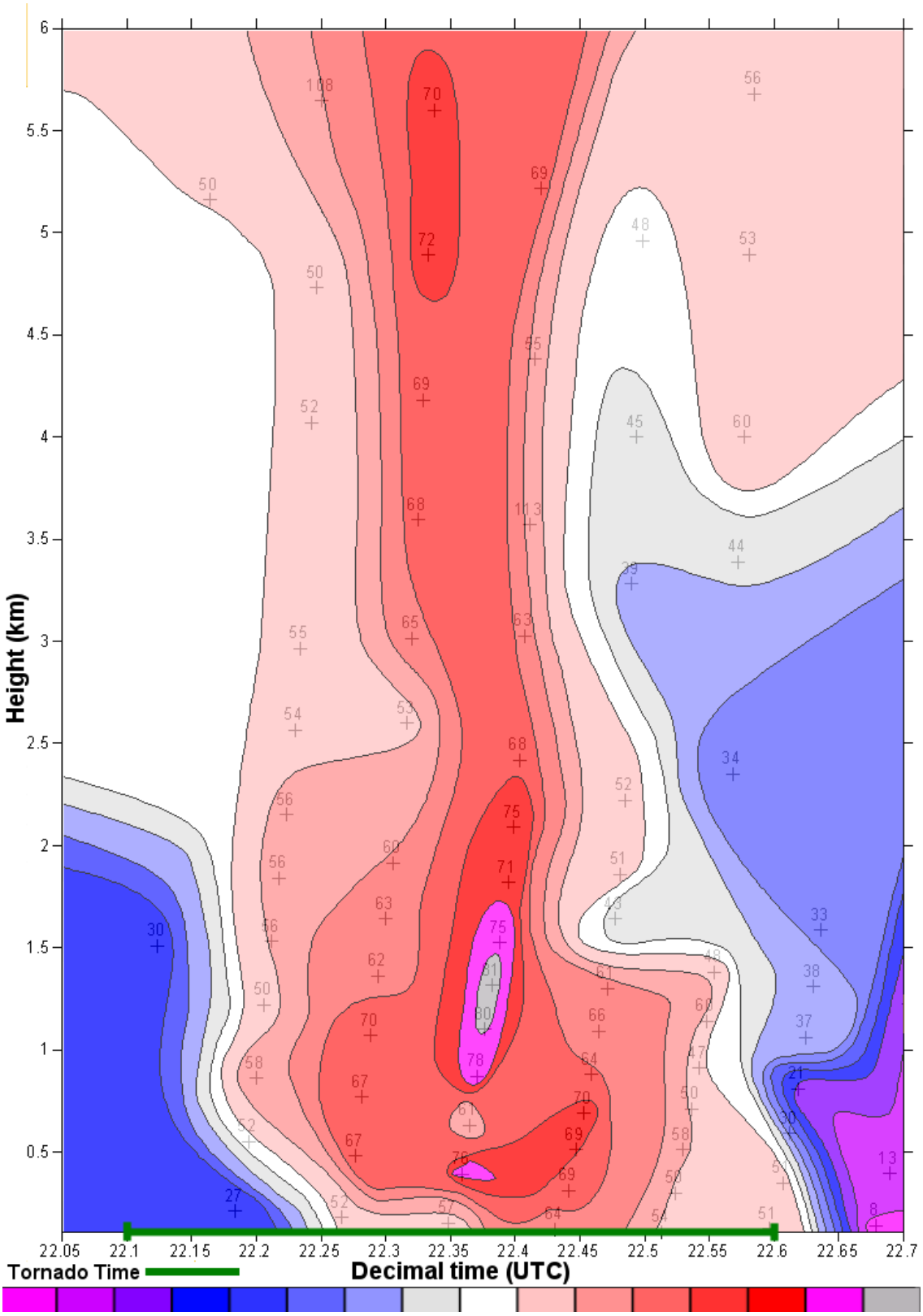

Figure 11. Time-height plot of TVS delta-V (m/s) for KTLX.
Shows TVS developing suddenly in all levels.

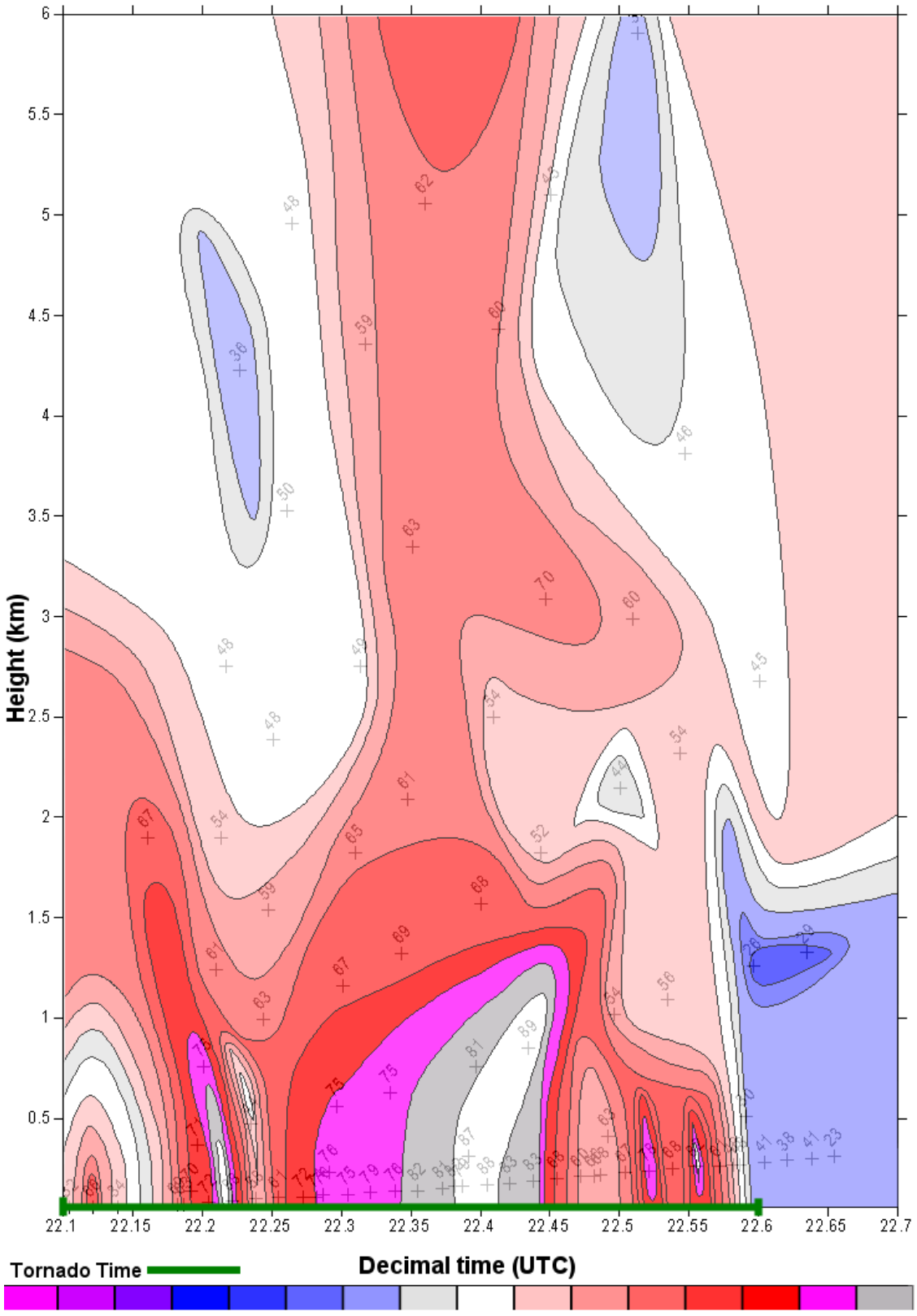

Figure 12. Same as figure 11 but for TDWR.
Shows TVS developing at the surface, ascending, then descending.

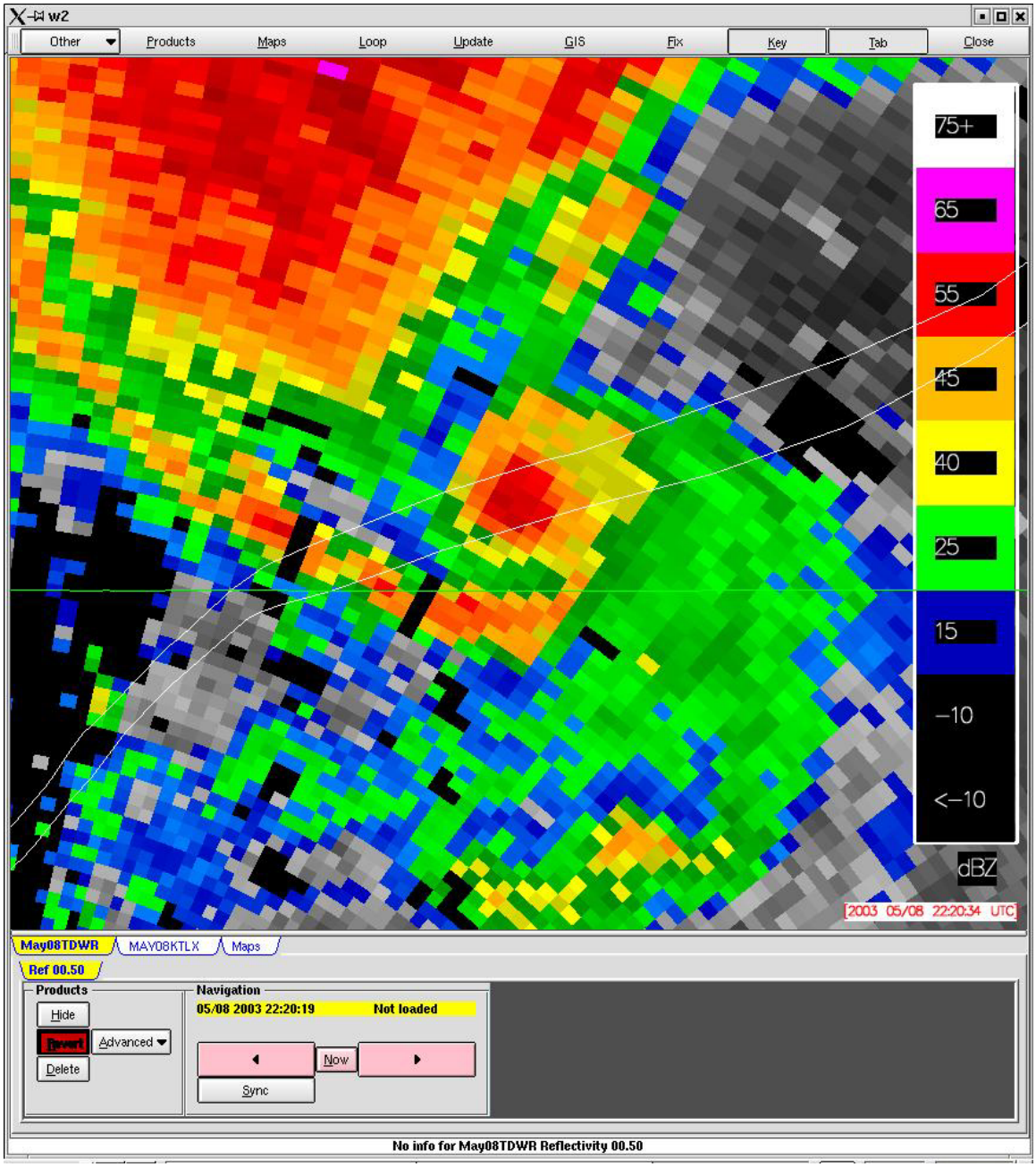

Figure 13. TDWR reflectivity "ball" associated with debris within the tornado and tornado cyclone circulation.

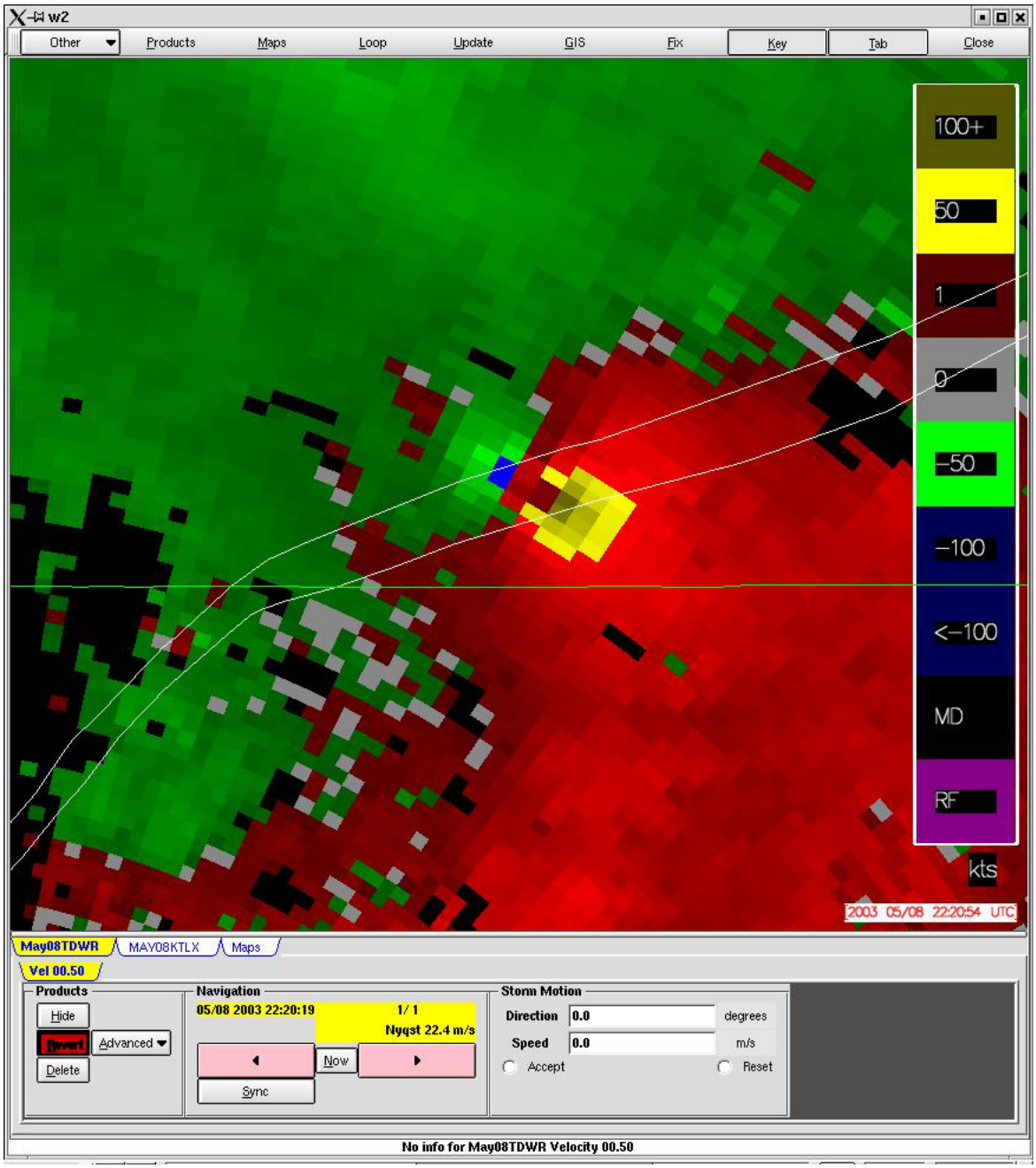

Figure 14. High-shear TDWR velocity couplet associated with tornado circulation (treated as TVS).

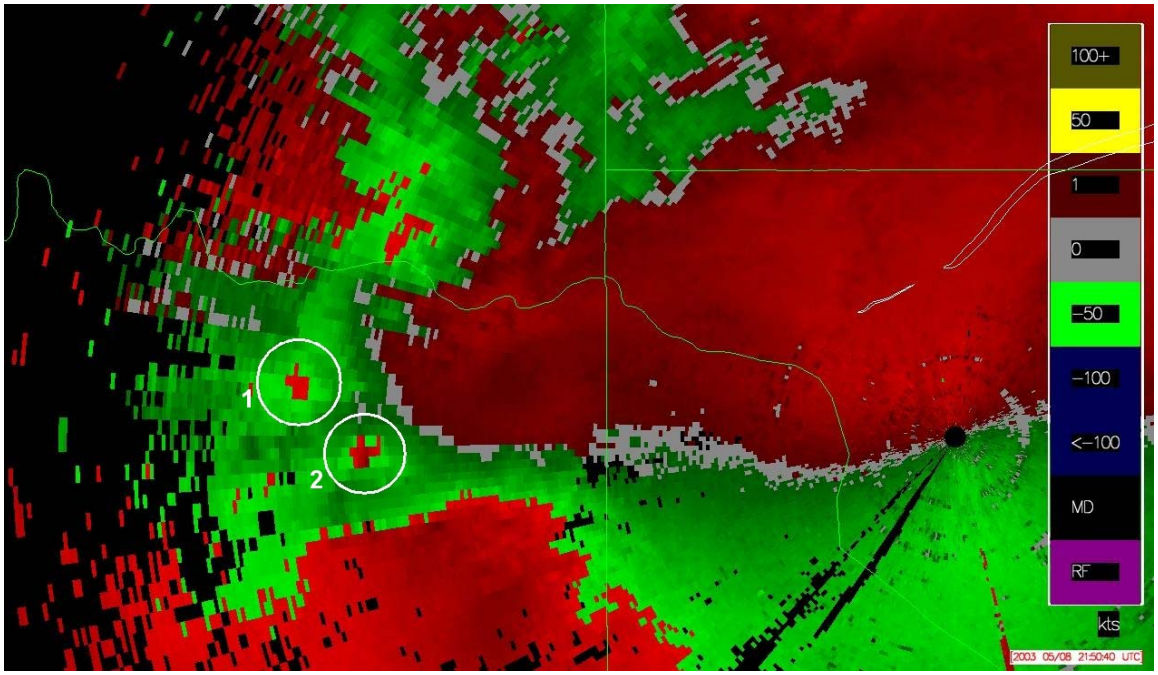

Figure 15. Screen capture of TDWR velocity data showing two RFD surges (circled) at the 5.1° elevation angle (~2.5 km AGL), 2151 UTC (451 PM CDT). The RFD surge labeled 2 is more recent.

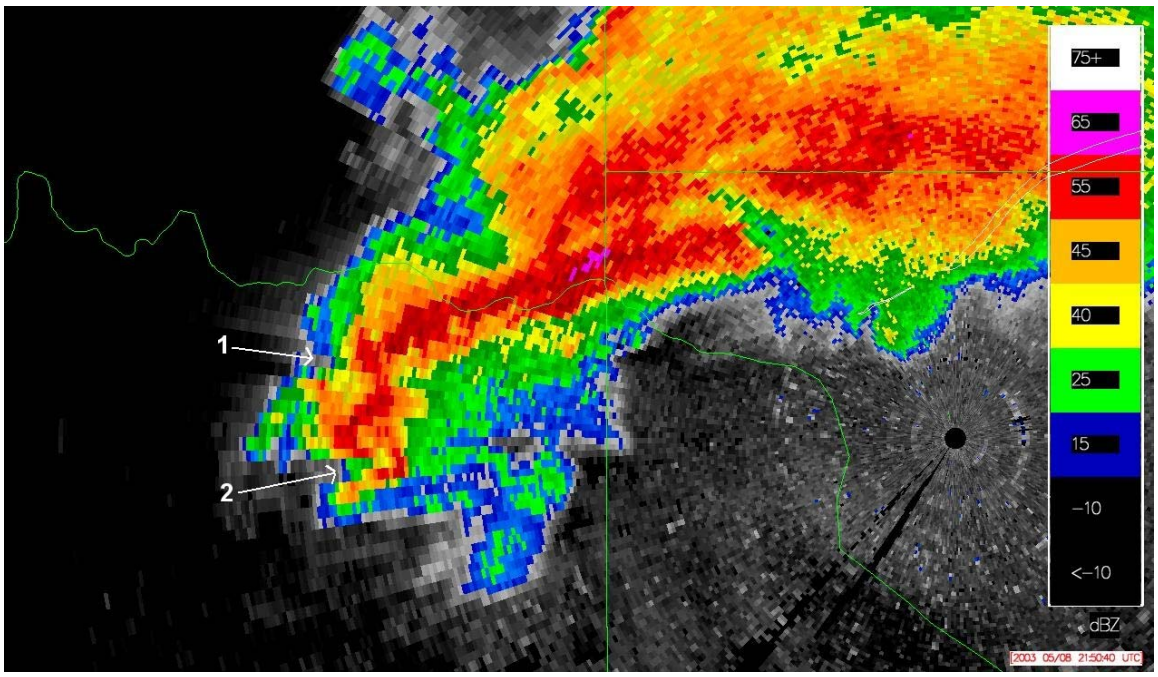

Figure 16. Same as figure 15 using reflectivity data. Each RFD surge is associated with a notch in reflectivity labeled with an arrow.